because of periodic relationships. A method exists for the production of HCO_3^- in the gas phase,[8] where several of its properties have been studied in the absence of solvent. We now report observation of the $HTiO_3^-$ ion by negative chemical ionization (NCI) mass spectrometry of titanium tetra-*n*-butoxide (Alfa Chemicals, Danvers, MA) and confirmation of the composition of the ion by its collisionally activated decomposition. Formation of such an ion was anticipated on the basis of prior experience with the formation of monomeric metaphosphate from several phosphate esters,[9] for in our experiments the negative ions have low internal energies and long lifetimes, qualities conducive to the formation of rearrangement products. NCI spectra were obtained on a ZAB-4F four-sector mass spectrometer[10] (BEEB geometry, VG Analytical Ltd., Manchester, U.K.) by introduction of the alkoxide via a partially retracted direct probe into a source at 75 °C with 5×10^{-6} torr Ar (as measured with the source ion gauge) as a buffer gas. Under these conditions the spectrum is dominated by ions from the more efficiently ionized halogen-containing impurities present in the sample from its preparation, but there is a peak of intensity 3% (relative to that of the most abundant negative ion in the spectrum, $(C_4H_9O)_2TiClO^-$; halogen-free ions are all of low abundance) present at *m/z* 97 with appropriate isotope peaks to contain one Ti. The charge of this ion was reversed by collision (after original acceleration through 7000 V) with thermal He (3×10^{-6} mbar) in a cell between the second and third sectors. The resulting collisionally activated decomposition (CAD) spectrum consisted of four peaks (percentages given are those of fragment ion current, uncorrected): *m/z* 64, 40%; *m/z* 65, 17%; *m/z* 80, 16%; *m/z* 81, 27%. These ions thus correspond to $^{48}TiO^+$, $^{48}TiOH^+$, $^{48}TiO_2^+$, and $^{48}TiO_2H^+$, by loss of the elements of HO_2, O_2, OH, and O, respectively, from the transitory[11] cation TiO_3H^+.

Structures were modeled by Fletcher–Powell geometry optimization using GAUSSIAN 82[15] and the Ti STO-3G basis set of Hehre.[16] A modification to facilitate convergence was added to the SCF module.[17] The geometry of the $HOTiO_2^-$ form of the anion, which we considered the most likely structure, was minimized by beginning with the Ti–O bonds and then the O–Ti–O angle, the distance from the O–Ti–O plane of the O bonded to H and Ti, the Ti–O–H angle, and the O–H bond length. The bond angles are then as follows: O–Ti–O, 123.9 ± 0.1°; Ti–O–H, 106.9 ± 0.1°; out of plane O (bonded to H and Ti) angle from the O–Ti–O plane, 6.8 ± 0.1°. The H–O–Ti plane bisects this latter O–Ti–O plane. The bond lengths are as follows: Ti–O, 166.1 ± 1 pm; Ti–OH, 191.4 ± 1 pm; O–H, 99.15 ± 1 pm. Since there is a report of a hydrido complex of a titanium(IV) alkoxide,[18] we also considered the form $HTi(O)_3^-$, with a Ti–H bond. Although numerous attempts were made, we could not obtain stable convergence for this form.

The experimental evidence speaks against the existence of the $HTi(O)_3^-$ form: there is no loss of H alone, as is virtually universally observed for H attached to a less electronegative atom. Formation of weak bonds like peroxy O–O bonds from species with stronger bonds is unprecedented in NCI chemistry, so that the forms $HOTi({=}O)OO^-$ and $HOO{-}Ti(O)_2^-$ are unlikely.

Thus calculations suggest that the structure $HOTiO_2^-$ exists in a potential well. Our observation of an ion of appropriate exact mass and of fragments at only the logical masses for the formula and structure confirm its existence for at least tens of microseconds in the absence of solvation.

One may at this point examine expected periodic relationships between HCO_3^- and $HTiO_3^-$, for they both are in old group IV, and assume that the only structural difference between HCO_3^- and $HTiO_3^-$ results from differences in the radii of C(IV) and Ti(IV). Data on HCO_3^- from the crystal structure of $NaHCO_3$[19] or from calculations of the free gaseous ion[8,20] both would have predicted a planar C_{2v} structure for $HTiO_3^-$. Use of the data from the crystal structure of HCO_3^- leads to the prediction of an O–Ti–O angle of 124° and Ti–O bond lengths of 180 and 188 pm; use of the computational results for the gas-phase ion would have generated 129° and 179 and 198 pm, respectively. The differences between this simple analogy and the result of the present computation are not so great, particularly when one considers the comparison with gas-phase HCO_3^-, where the elongated C–OH bond (relative to the bond length in the crystal structure) has drawn some attention.[20] The same pattern of elongation appears in the Ti–OH ion, and indeed the differences between the simplistic model and the computed structure are merely the modest nonplanarity and the somewhat shorter bond lengths of the latter. Our observation of $HTiO_3^-$ and computation of its structure, then, permits some delineation of the degree of periodic relationships in old groups IVA and IVB.

Registry No. $HTiO_3^-$, 98943-14-7; titanium tetra-*n*-butoxide, 5593-70-4.

---

(8) R. G. Keesee, N. Lee, and A. W. Castleman, Jr., *J. Am. Chem. Soc.*, **101**, 2599 (1973).

(9) D. J. Harvan, J. R. Hass, K. L. Busch, M. M. Bursey, F. Ramirez, and S. Meyerson, *J. Am. Chem. Soc.*, **101**, 7409 (1979).

(10) J. R. Hass, B. N. Green, R. H. Bateman, and P. A. Bott, submitted for publication.

(11) The main beam of the charge-reversed ion was not observed. This has precedent in charge reversal of other anions.[12-14]

(12) M. M. Bursey, D. J. Harvan, C. E. Parker, and J. R. Hass, *J. Am. Chem. Soc.*, **101**, 5485 (1979).

(13) M. M. Bursey, D. J. Harvan, C. E. Parker, L. G. Pedersen, and J. R. Hass, *J. Am. Chem. Soc.*, **101**, 5489 (1979).

(14) T. A. Lehman, M. M. Bursey, and J. R. Hass, *Org. Mass Spectrom.*, **18**, 375 (1983).

(15) J. S. Brinkley, M. J. Frisch, D. J. Defrees, K. Ragavachari, R. A. Whiteside, H. B. Schlegel, E. M. Fluder, and J. A. Pople, "GAUSSIAN 82", copyright Carnegie-Mellon University, Pittsburgh, PA, 1983.

(16) W. J. Pietro and W. J. Hehre, *J. Comput. Chem.*, **4**, 241 (1983).

(17) D. Poppinger, personal communication.

(18) T. Kuratsuji, T. Urasaki, and W. Funakoshi, *Jpn. Pat.* JP 51/140992, Dec 4, 1976; *Chem. Abstr.*, **86**, 90879*w* (1977).

(19) R. L. Sass and R. F. Scheuermann, *Acta Crystallogr.*, **15**, 77 (1962).

(20) B. Jönsson, G. Karlström, and H. Wennerström, *J. Am. Chem. Soc.*, **100**, 1658 (1978).

Contribution from AT&T Bell Laboratories,
Murray Hill, New Jersey 07974

Formation of Polynuclear Chlorometalates by the Reduction of Transition-Metal Chlorides with Samarium Metal Slurries: Preparation and EXAFS Structure of $SmNb_3Cl_{14}$

A. P. Ginsberg*[†] and A. L. Wayda*

Received March 25, 1985

High-temperature reduction of early-transition-metal halides with metals has been a key technique for the synthesis of metal–metal-bonded polynuclear metal halides.[1] The possibility that similar reactions might take place under mild conditions if the metal reducing agent were in a highly active form has prompted us to investigate the reaction of metal-atomization-generated metal slurries[2] in hydrocarbons with early-transition-metal halides. In this communication we report that samarium metal slurries in methylcyclohexane reduce Nb_2Cl_{10}, Ta_2Cl_{10}, and $TiCl_4$ to form new polynuclear chlorometalate anions. In particular, we describe the characterization of the compound $SmNb_3Cl_{14}$, which contains a linear trinuclear mixed-valance chloroniobate anion.

Samarium metal slurry was prepared by cocondensing samarium metal with methylcyclohexane at liquid-nitrogen temperature in a Planer metal vapor apparatus.[3] After it was warmed to room temperature, the pyrophoric slurry was transferred under argon to a Schlenk tube. The final slurry contained ~10 mg of Sm/mL. Reactions with the metal chlorides were carried out in an He-filled Vacuum Atmospheres glovebox by stirring a portion of the slurry with a large excess of the metal chloride, either neat

---

[†] Correspondence should be addressed to P.O. Box 986, New Providence, NJ 07974.

0020-1669/85/1324-4749$01.50/0

Table I. Reactions of Sm Metal Slurry with Excess Metal Halide at Room Temperature

metal halide	reacn time	product[a]	color
$TiCl_4$[b]	12 h	$Sm_2Ti_3Cl_{13}\cdot 0.75CH_3C_6H_{11}$	YBr
$TiCl_4$[b]	5 days	$Sm_2Ti_2Cl_9\cdot 0.65CH_3C_6H_{11}$	Br
Nb_2Cl_{10}[c,d]	4 days	$SmNb_3Cl_{14}\cdot 0.3CH_3C_6H_5$[e]	RBr
Ta_2Cl_{10}[c]	4 days[f]	$SmTa_2Cl_9\cdot 0.75CH_3C_6H_5$	Br

[a] The products all appeared homogeneous on microscopic examination. Complete elemental microanalyses (Analytische Laboratorien, Engelskirchen, West Germany) are in satisfactory agreement with the indicated stoichiometries. The absence of a band at 220 cm^{-1} in the infrared spectra (CsI disk) of these compounds shows that they do not contain $SmCl_3$. In the case of the Nb complex, the magnetic susceptibility measurements demonstrate the absence of $SmCl_2$. [b] Neat. [c] In toluene solution. [d] 40-mesh Sm powder does not react with Nb_2Cl_{10} in toluene even after ultrasonication for several days. [e] Mass spectrometry at 100 °C confirms the presence of toluene. [f] After 4 days at room temperature this reaction was heated at reflux for 12 h.

($TiCl_4$) or in toluene solution ($NbCl_5$, $TaCl_5$) for 0.5–5 days. The metal reacted completely, and the product that precipitated was washed with toluene and methylcyclohexane and then pumped for 12 h at room temperature (10^{-6} mmHg). Table I summarizes these experiments. The products are all very air- and moisture-sensitive.

The chlorometalates in Table I have not been reported previously. $Ta_2Cl_9{}^{n-}$ in $SmTa_2Cl_9$ is presumably analogous to the known $Nb_2Cl_9{}^{3-}$ anion, a d^2–d^2 dimer with the confacial-bioctahedral structure and a $\sigma^2\pi^2$ Nb–Nb double bond.[4] $Ti_2Cl_9{}^{n-}$ in $Sm_2Ti_2Cl_9$ is probably a reduced form of the known $Ti_2Cl_9{}^{3-}$ anion.[5]

Magnetic susceptibility measurements on $SmNb_3Cl_{14}$ over the temperature range 282–99 K show that the sample has a temperature-dependent magnetic moment which decreases from $\mu_{eff} = 1.60\ \mu_B$ at 281.9 K to 1.14 μ_B at 99.5 K. Comparison with the theoretical equations given by Van Vleck[6] for Sm demonstrates that the observed susceptibility is due entirely to Sm^{3+} and that therefore the chloroniobate anion contains no unpaired spins.

Lacking single crystals, we have investigated the structure of $SmNb_3Cl_{14}$ by extended X-ray absorption fine structure (EXAFS) spectroscopy, a powerful technique for studying the immediate environment around an X-ray-absorbing atom.[7] EXAFS fluorescence[8] measurements were carried out at the Cornell High Energy Synchrotron Source (CHESS) on the C2 beam line.[9] Data collection, reduction, and analysis were performed as described in the literature.[10-12] Figure 1a shows the Fourier transform of the normalized background-corrected Nb K-edge EXAFS spectrum. The peaks at 1.82, 2.20, and 2.69 Å are assigned, respectively, to terminal Nb–Cl, bridging Nb–Cl, and Nb–Nb bonds. The distances r' in Figure 1a differ from the true distances r by a phase shift $\delta = r - r'$. From the EXAFS spectrum of the model compound Nb_2Cl_{10} we obtain the following approximate values for δ: Nb–Cl, 0.5 Å; Nb···Nb, 0.3 Å. Transferring these phase shifts to $SmNb_3Cl_{14}$ gives the following corrected distances: $Nb–Cl_{ter}$ = 2.3 Å, $Nb–Cl_{br}$ = 2.7 Å, and Nb–Nb = 3.0 Å. More accurate results are provided by the curve-fitting analysis discussed below.

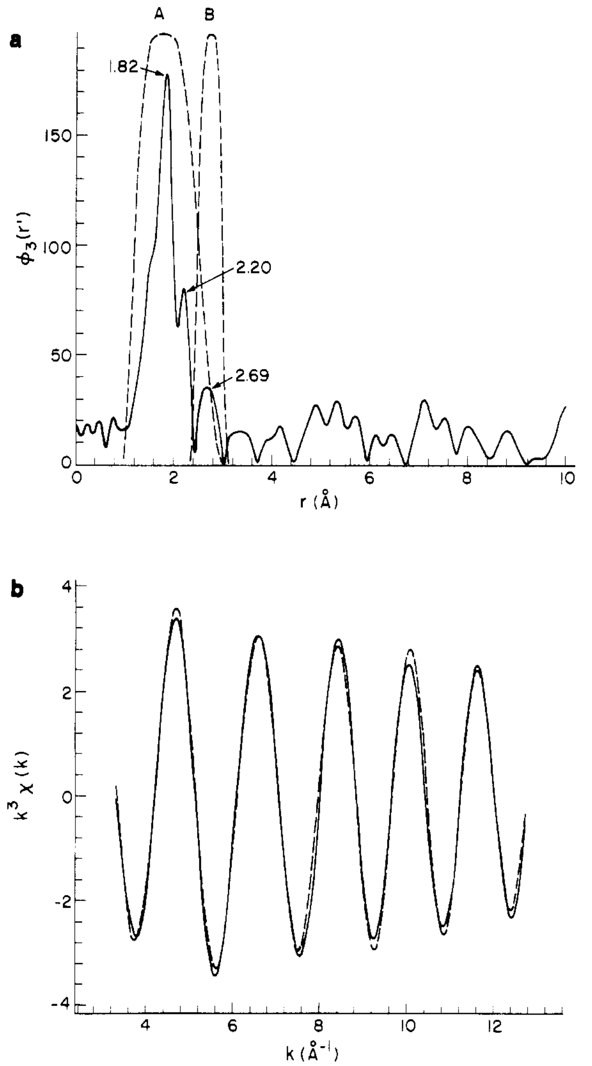

Figure 1. (a) Fourier transform of the normalized background-subtracted $k^3[\chi(k)]$ vs. k Nb K-edge EXAFS spectrum of $SmNb_3Cl_{14}$. The dashed curves are the filtering windows for (A) the Nb–Cl peaks and (B) the Nb–Nb peak. (b) The Fourier-filtered (filter A) back-transformed Nb EXAFS spectrum (solid curve) and the two-term (Nb–Cl, Nb–Cl) nonlinear least-squares fit to eq 1 (dashed curve).

---

(1) Corbett, J. D. *Acc. Chem. Res.* **1981**, *14*, 239.

(2) Klabunde, K. J.; Efner, H. F.; Satek, L.; Donley, W. *J. Organomet. Chem.* **1974**, *71*, 309. Klabunde, K. J.; Efner, H. F.; Murdock, T. O.; Ropple, R. *J. Am. Chem. Soc.* **1976**, *98*, 1021. Davis, S. C.; Klabunde, K. J. *Am. Chem. Soc.* **1978**, *100*, 5973.

(3) G. V. Planer Ltd., Middlesex, England.

(4) Broll, A.; von Schnering, H. G.; Schäefer, H. *J. Less-Common Met.* **1970**, *22*, 243.

(5) Saillant, R.; Wentworth, R. A. *Inorg. Chem.* **1968**, *7*, 1606.

(6) Van Vleck, J. H. "The Theory of Electric and Magnetic Susceptibilities," Oxford University Press: London, 1932; pp 245–253.

(7) See, for example: "EXAFS Spectroscopy"; Teo, B. K., Joy, D. C., Eds.; Plenum Press: New York, 1981.

(8) Jaklevic, J.; Kirby, J. A.; Klein, M. P.; Robertson, A. S.; Brown, G. S.; Eisenberger, P. *Solid State Commun.* **1977**, *23*, 679.

(9) Batterman, B. W.; Ashcroft, N. W. *Science (Washington, D.C.)* **1979**, *206*, 157. See also: Batterman, B. W. In ref 7, pp 197–203.

(10) (a) Eisenberger, P.; Kincaid, B. M. *Science (Washington, D.C.)* **1978**, *200*, 1441. (b) Lee, P. A.; Citrin, P. H.; Eisenberger, P.; Kincaid, B. M. *Rev. Mod. Phys.* **1981**, *53*, 769. (c) Teo, B. K. In ref 7, pp 13–58. (d) Teo, B. K.; Antonio, M. R.; Averill, B. A. *J. Am. Chem. Soc.* **1983**, *105*, 3751.

(11) Finely divided samples of $SmNb_3Cl_{14}$ and Nb_2Cl_{10} were dispersed in layers of pressed boron nitride and sealed in aluminum cells with 1-mil Kapton tape; the cells were surrounded by a nitrogen atmosphere during the measurements. Nb K-edge (threshold energy (E_0) 18985 eV) fluorescence EXAFS spectra were collected at ambient temperature in steps of constant **k** (photoelectron wave vector) from about 100 eV below to about 900 eV above the absorption edge. The raw data consisted of the ratio of fluorescent to incident photointensity (I_f/I_0) as a function of E, the incident X-ray photon energy.

(12) EXAFS data reduction was carried out with Bell Laboratories programs developed by B. M. Kincaid and consisted of the following steps: The I_f/I_0 data were converted from E to **k** space and multiplied by $\mathbf{k}^3$, by using the definition equation $\mathbf{k} = [2m/\hbar^2(E - E_0)]^{1/2}$. A smooth background correction was subtracted from the data by means of a cubic spline technique, and the results were divided by the background correction to give $\mathbf{k}^3[\chi(\mathbf{k})]$, where $\chi(\mathbf{k})$ is the fractional modulation of the X-ray absorption coefficient due to EXAFS. Fourier transformation of the $\mathbf{k}^3[\chi(\mathbf{k})]$ vs. **k** data gave the radial distribution function $\phi_3(r')$ in distance (r') space. High-frequency noise and the small residual background in the spectra were removed by Fourier filtration in which the product of $\phi_3(r')$ with a smooth filter window on a selected r' range was Fourier back-transformed to **k** space. The filtered data, after truncation at 3 and 13 Å, were subjected to least-squares curve-fitting analysis.

Table II. Least-Squares-Refined Parameters and Estimated Standard Deviations (in Parentheses)[a] from Best Fits of Eq 1 to EXAFS Spectra of $SmNb_3Cl_{14}$ and Nb_2Cl_{10}

		best-fit parameters				model-adjusted results[b]		expected[c] results		
compd	term	ΔE_0, eV	r, Å	σ, Å	B	r, Å	N	r, Å	N(I)	N(II)
$SmNb_3Cl_{14}$	Nb–Cl_{ter}	−0.93	2.309 (15)	0.097 (7)	2.61	2.324 (8)	3.2 (7)	2.30	3.33	2.00
	Nb–Cl_{br}	−10.87	2.509 (15)	0.048 (39)	0.87	2.552 (25)	2.4 (20)[d]	2.42–2.55	2.67	4.00
	Nb–Nb	−5.70	3.051 (19)	0.043 (31)	0.14	3.042 (9)	0.7 (4)	3.03	1.33	1.33
Nb_2Cl_{10}	Nb–Cl_{ter}	−0.82	2.263 (7)	0.037 (15)	1.30			2.302 (5)	4	
	Nb–Cl_{br}	−7.06	2.544 (29)	0.070[e]	0.59			2.555 (6)	2	
	Nb–Nb	−9.54	3.935 (17)	0.079 (16)	0.52			3.951 (2)	1	

[a] Standard deviations were estimated as in ref 10d and do not include possible systematic errors. [b] The best-fit values of r were corrected by the FABM method as described by Teo et al.[10d] The coordination numbers N were calculated from the best-fit values of B by using amplitude reduction factors S obtained from the B(Nb–Cl_{ter}) and B(Nb–Nb) vs. σ correlation curves of Nb_2Cl_{10} at the best-fit σ values for $SmNb_3Cl_{14}$. [c] For $SmNb_3Cl_{14}$ the expected values refer to structures I and II; the X-ray results for Nb_2Cl_{10} are from ref 16. [d] The very large uncertainty of this result is due to the insensitivity of the fit to the values of the strongly coupled parameters σ_{br} and B_{br}. [e] The fit is extremely insensitive to the value of this Debye–Waller factor; it was held fixed at the value calculated[10c] from the Nb–Cl_{br} stretching frequency (248 cm^{-1}).

A nonlinear least-squares procedure[13] was used to fit the Fourier-filtered, truncated $\mathbf{k}^3[\chi(\mathbf{k})]$ vs. $\mathbf{k}$ EXAFS data[12] with the single scattering short-range order theory equation[10,14]

$$\mathbf{k}^3[\chi(\mathbf{k})] = \sum_j B_j[F_j(\mathbf{k}_j)]\mathbf{k}_j^2 \exp(-2\sigma_j^2\mathbf{k}_j^2) \sin\,[2\mathbf{k}_j r_j + \phi_j(\mathbf{k}_j)]/r_j^2 \quad (1)$$

where $F_j(\mathbf{k}_j)$, $\phi_j(\mathbf{k}_j)$, σ_j, r_j, and $\mathbf{k}_j$ represent the backscattering amplitude, the total photoelectron phase shift, the Debye–Waller factor, the distance from the absorbing atom, and the photoelectron wave vector, respectively, for a neighboring atom of type j. B_j is a scale factor related to N_j, the number of j-type neighbor atoms, by $N_j = B_j/S_j$; the amplitude reduction factor S_j was evaluated from the model compound EXAFS spectrum. $F_j(\mathbf{k}_j)$ and $\phi_j(\mathbf{k}_j)$ were fixed at their theoretical values during the least-squares fitting.[15] Wave vectors $\mathbf{k}$ and $\mathbf{k}_j$ are related by[15]

$$\mathbf{k}_j = (\mathbf{k}^2 - 2(\Delta E_{0j})/7.62)^{1/2}$$

where $\Delta E_{0j} = E_{0j}^{theor} - E_0^{exptl}$ is the difference between the experimental absorption edge threshold energy[11] and the threshold energy for which the theoretical $\phi_j(\mathbf{k}_j)$ function is defined. There are therefore four parameters, r_j, ΔE_{0j}, σ_j, and B_j, to be least-squares refined for each term of eq 1. Figure 1b shows the Fourier-filtered Nb–Cl EXAFS spectrum and the least-squares fit to eq 1 with two terms. The Nb–Nb peak was filtered and fit with one term of eq 1. Table II summarizes the results of the least squares analyses.

The results in Table II are consistent with the formulation $Sm^{3+}[Nb_3Cl_{14}]^{3-}$ and a structure comprised of a chain of three $NbCl_6$ octahedra sharing common edges (I). They are also consistent with the formulation $Sm^{3+}[Nb_3Cl_{12}]^-Cl^-_2$ and a structure comprised of a chain of three $NbCl_6$ octahedra sharing common faces (II). The short Nb–Nb bond accounts for the diamagnetism of $[Nb_3Cl_{14}]^{3-}$ or $[Nb_3Cl_{12}]^-$, which may be represented as containing Nb in the oxidation states IV(d^1)–III(d^2)–IV(d^1) with the spins paired in $\sigma^2\pi^2$ metal–metal bonds. Each Nb–Nb pair has a bond order of 1, consistent with the observed Nb–Nb distance. A triangular $[Nb_3Cl_{12}]^-$ cluster would have a bond order of $^2/_3$ and would be expected to have a longer Nb–Nb distance than is observed. The $[Nb_3Cl_{14}]^{3-}$ structure is related to the structure of $NbCl_4$.[17] The latter compound contains linear chains of edge-sharing $NbCl_6$ octahedra in which long (3.794 (2) Å) and short (3.029 (2) Å) Nb–Nb distances alternate; the bonded Nb–Nb pairs are linked by a single σ bond. Although the short Nb–Nb distance in $NbCl_4$ is close to the distance in $[Nb_3Cl_{14}]^{3-}$, the corresponding Nb–Cl_{br} distance (2.425 (1) Å) is significantly shorter than this distance in $[Nb_3Cl_{14}]^{3-}$.[18] The Nb–Cl_{ter} distance in $[Nb_3Cl_{14}]^{3-}$ is significantly longer than the distance in $NbCl_4$ (2.291 (2) Å). However, we note that there is probably an appreciable spread between nonequivalent Nb–Cl_{ter} distances. This is indicated by the large value found for the Debye–Waller factor of the Nb–Cl_{ter} bond, which suggests a distance spread of ~0.1 Å[10c,19] and the possibility of significant Sm–Cl interactions.

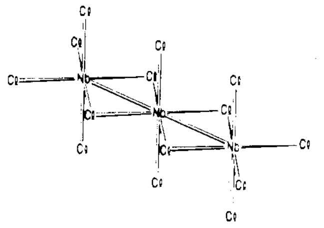

I

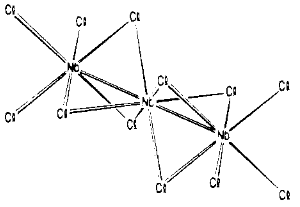

II

Acknowledgment. We are very much indebted to Dr. B. K. Teo for educating us in the art of measuring and analyzing EXAFS spectra. We thank Prof. D. F. Shriver for his help and Peter Blonsky for his aid in operating the EXAFS spectrometer.

---

(13) A Bell Labs fitting program based on Marquardt's method.

(14) Stern, E. A. *Phys. Rev. B: Solid State* **1974**, *10*, 3027. Lee, P. A.; Pendry, J. B. *Phys. Rev. B: Solid State* **1975**, *11*, 2795. Lee, P. A.; Beni, G. *Phys. Rev. B: Solid State* **1977**, *15*, 2862.

(15) Teo, B. K.; Lee, P. A. *J. Am. Chem. Soc.* **1979**, *101*, 2815.

(16) Zalkin, A.; Sands, D. E. *Acta Crystallogr.* **1958**, *11*, 615.

(17) Taylor, D. R.; Calabrese, J. C.; Larsen, E. M. *Inorg. Chem.* **1977**, *16*, 721.

(18) The corresponding Cl_{br}–Nb–Cl_{br} angles are 106.8° in $[Nb_3Cl_{14}]^{13-}$ and 102.7° in $NbCl_4$.

(19) Teo, B. K.; Shulman, R. G.; Brown, G. S.; Meixner, A. E. *J. Am. Chem. Soc.* **1979**, *101*, 5624.

Contribution from the Department of Chemistry,
University of Virginia, Charlottesville, Virginia 22901

Solvent-Induced ^{11}B NMR Shifts in Metallaboranes and Metallacarboranes

T. Leon Venable,[1a] Cynthia T. Brewer,[1b] and Russell N. Grimes*

Received March 26, 1985

Although the effect of solvent on proton NMR spectra of boron cage compounds has been examined,[2] and Onak et al. have correlated solvent shifts with proton charges,[2a] the ^{11}B NMR spectra of polyhedral boranes and carboranes are usually assumed to be negligibly affected by the choice of solvent, with observed solvent shifts normally much less than 1 ppm and measurable only on high-resolution instruments.[3] A recently noted exception[4] is

---

(1) (a) Present address: Department of Chemistry, Agnes Scott College, Decatur, GA 30030. (b) Excerpted in part from: Brewer, C. T. Ph.D. Thesis, University of Virginia, 1984.

(2) (a) Onak, T.; Inman, W.; Rosendo, H.; DiStefano, E. W.; Nurse, J. *J. Am. Chem. Soc.* **1977**, *99*, 6488. (b) Jarvis, W.; Inman, W.; Powell, B.; DiStefano, E. W.; Onak, T. *J. Magn. Reson.* **1981**, *43*, 302.

0020-1669/85/1324-4751$01.50/0